



Burst-mode femtosecond fiber-feedback optical parametric oscillator

MORITZ FLOESS,*  TOBIAS STEINLE, AND HARALD GIESSEN 

4th Physics Institute and Stuttgart Research Center of Photonic Engineering, University of Stuttgart, Pfaffenwaldring 57, 70569 Stuttgart, Germany

*Corresponding author: m.floess@pi4.uni-stuttgart.de

Received 27 October 2021; revised 10 December 2021; accepted 14 December 2021; posted 17 December 2021; published 20 January 2022

In multiphoton 3D direct laser writing and stimulated Raman scattering applications, rapid and arbitrary pulse modulation with an extremely high contrast ratio would be very beneficial. Here, we demonstrate a femtosecond fiber-feedback optical parametric oscillator (FFOPO) system in combination with pulse picking in the pump beam. This allows tunable signal output at variable burst rates from DC all the way up to 5 MHz. Furthermore, arbitrary pulse sequences can be generated. The rapid signal buildup dynamics provide individual full-power pulses with only two prepulses. This is possible without the requirement for additional injection seeding. Hereby, the intrinsically high intra-cavity losses of the FFOPO system are found to be beneficial, as they enable rapid off-switching of the output as signal ring-down is efficiently suppressed. Possible applications are the reduction of the average power while maintaining a high peak power level, as well as tunable arbitrary pulse sequence generation. © 2022 Optica Publishing Group

<https://doi.org/10.1364/OL.446933>

Introduction. Pulse picking finds numerous applications wherever it is necessary to reduce the repetition rate of a pulsed laser. There may, for instance, be a need to solely pick individual pulses or to generate pulse bursts. In particular, multi-photon direct laser writing benefits from variable pulse repetition rates and burst operation while the pulse energy is kept constant. The spatial resolution of 3D two-photon polymerization writing can be increased by applying femtosecond pulse bursts with pulse energies of a few nanojoules rather than a steady pulse train, since local heat accumulation is minimized [1]. Heat-induced micro-explosions in the photoresist can be avoided by choosing appropriate pulse sequences [2]. Similarly, the fabrication of integrated optical components using femtosecond laser pulses benefits from burst operation. In this case, avoiding or deliberately introducing heat accumulation enables control over the resulting morphology and optical properties [3,4]. Also, reducing the repetition rate of the laser is often important for time-resolved fluorescence spectroscopy, where long lifetimes of molecules require quite large temporal pump-pulse separation [5,6].

Furthermore, coherent laser spectroscopy modalities that are based on lock-in detection rely on laser modulation. For example, stimulated Raman scattering spectroscopy requires amplitude

modulation of one of the interacting laser pulse trains [7–11], which is usually realized by employing an acousto-optical modulator (AOM). AOMs suffer from wavelength-dependent modulation efficiency with typical maximum modulation depths of approximately 80% in the zeroth diffraction order. Operation in the first diffraction order enables 100% modulation but imposes a reduced maximum power level as well as wavelength-dependent diffraction angles.

In this work, we avoid these problems by combining pulse picking with a subsequent synchronously pumped fiber-feedback optical parametric oscillator (FFOPO). Instead of placing the AOM in the signal output beam, pulse picking is performed in front of the FFOPO in the pump beam. This configuration is advantageous as the wavelength-dependent modulation performance of the AOM is removed from the system.

Parametric fluorescence, the random starting point for optical parametric oscillation, exhibits a strong timing jitter, which limits the effective gain due to a synchronization mismatch. Nevertheless, our system exhibits extremely fast buildup dynamics due to an amplification (small signal) gain of approximately 50 dB in the nonlinear crystal for the synchronized case. As a result, the signal pulse train reaches its steady-state pulse energy within only five pump cycles without any additional injection seeding. Additionally, high resonator losses originating from fiber incoupling and a high output coupling ratio are beneficial for rapid signal turnoff, which enables burst rates of up to 5 MHz. Other burst-mode OPO systems reported in the literature exhibit transients that extend across up to 80 pump cycles [12] and, thus, lack modulation bandwidth.

Setup. The FFOPO is synchronously pumped by an Yb:KGW oscillator that generates 1032 nm, 450 fs pulses at a repetition rate of 41 MHz and 8 W of average output power [13], as depicted in Fig. 1. An AOM is placed in the pump beam to act as a pulse picker. The AOM operates in the first diffraction order to ensure the highest possible suppression ratio of undesired laser pulses. The driver electronics for the AOM are synchronized to the pump laser. A frequency divider based on a field-programmable gate array (FPGA) sets the time base by shifting the pump laser repetition rate down. A programmable arbitrary waveform generator (UHF-AWG, Zurich Instruments) drives the AOM. This allows the generation of arbitrary pump pulse sequences. The FFOPO system is singly resonant for the signal channel and based on a 10-mm-long, 0.5-mm-thick periodically poled MgO:LiNbO₃ (PPLN) crystal with discrete poling

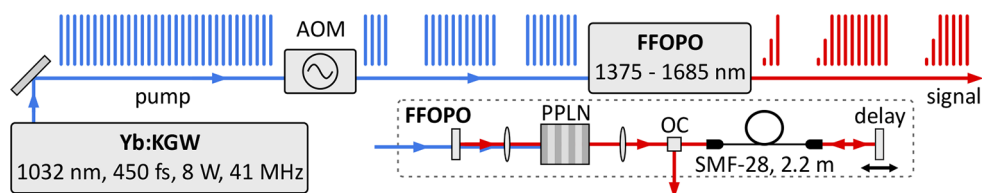


Fig. 1. Schematic of the setup. An Yb:KGW oscillator synchronously pumps a MgO:PPLN-based FFOPO at 41 MHz repetition rate. The inset depicts the linear cavity design, which incorporates a 2-m-long SMF-28 fiber and a variable-output coupler. An AOM allows the arbitrary generation of pump pulse sequences, each of which drives the FFOPO from its off state into its steady state within only a few cycles.

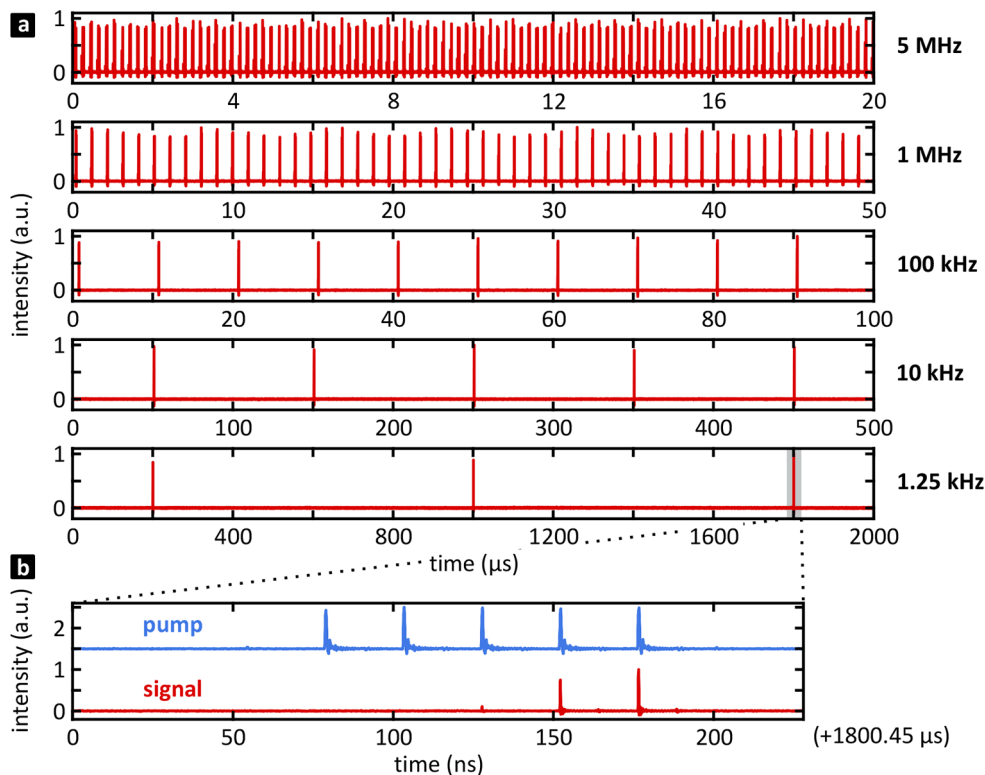


Fig. 2. (a) FFOPO signal output at five different burst rates between 1.25 kHz and 5 MHz, as measured at 1470 nm. (b) Zoom of the gray-shaded area in (a). The signal reaches the steady-state pulse energy within five pump cycles, which results in a signal pulse burst that consists of two prepulses followed by the main pulse. This rapid signal buildup enables burst rates of up to approximately 5 MHz. The high intra-cavity losses enable rapid turn-off of the signal output without any ring-down. Pump power: 680 mW (unmodulated); output coupling ratio: 94%.

periods and anti-reflection coatings at both facets ($R < 2\%$ at 1030 nm, $R < 3\%$ at 1350–1900 nm). The largest share of the FFOPO cavity is wound up in a 2.2-m-long feedback fiber with an effective propagation length of 4.4 m due to the double-pass configuration used. This imposes a large amount of intra-cavity group-delay dispersion on the signal feedback. The resulting chirp makes the pump–seed overlap insensitive to cavity mismatch fluctuations, and thus enables excellent long-term power and wavelength stability [14]. Even though only a narrow-bandwidth portion of the feedback is therefore available as the seed for the amplification process, the FFOPO generates signal pulses with 350 fs duration [14,15], which is governed by the nonlinear temporal gain window of the pump (450 fs) in combination with the gain bandwidth. The phase matching is tuned by changing the poling period and the temperature of the PPLN crystal. A moveable end mirror is employed to change the signal wavelength. A variable output coupler allows the

adjustment of the intra-cavity signal power in order to optimize the signal buildup time and the output power level. The signal output pulse trains are recorded using a 5 GHz InGaAs photodiode.

Results and discussion. Variable pulse burst rates are demonstrated in Fig. 2(a). The burst rate is varied from 5 MHz down to 1.25 kHz, measured at a signal wavelength of 1470 nm. The pump power level is set to 680 mW, measured at 41 MHz. In principle, there is no lower limit to the burst rate. In this case, the home-made FPGA-based trigger electronics set the lower limit to 1.25 kHz. Figure 2(b) depicts a temporal zoom into one of the signal pulse bursts as well as the corresponding pump burst. The feedback ratio is optimized to 6%, so only five pump pulses are required to drive the FFOPO into its steady state. Gain saturation sets in between pulse sites 4 and 5, which results in only minor amplification. This occurs without any additional

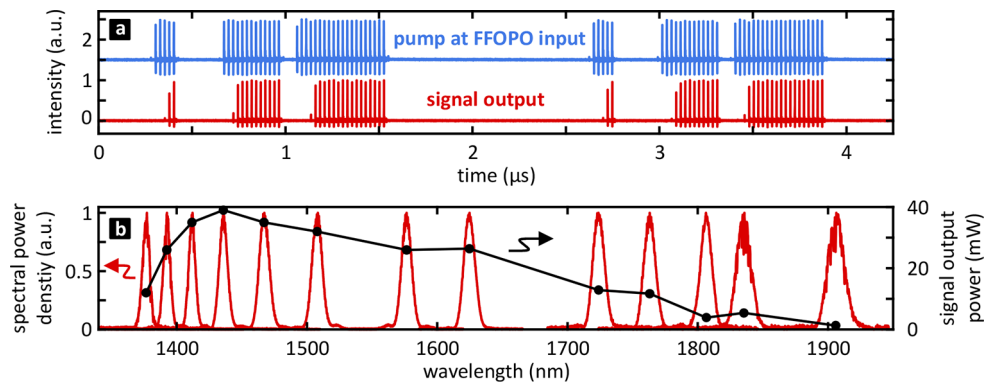


Fig. 3. (a) An arbitrary pump burst sequence drives the FFPO. (b) The spectral tunability of the signal output (left y axis) is depicted, as is the corresponding average signal output power (right y axis). Both the spectra and the output power were recorded while the FFPO was driven by the pulse sequence shown in (a). The measured signal output power therefore corresponds to a duty cycle of approximately 27%. The spectrum at 1410 nm corresponds to the signal burst sequence in (a). Pump power: 680 mW (unmodulated); output coupling ratio: 40–97% (optimized for maximum signal output).

injection seeding of the buildup process, which keeps the setup simple and cost efficient.

The fiber-feedback design imposes high intra-cavity losses, mainly caused by the limited fiber incoupling efficiency. In fact, this low Q-factor is advantageous, as it suppresses signal ring-down after the pump beam has been turned off, meaning that the signal output can be completely switched off within one cycle. Thus, skipping only a few pump cycles is sufficient to empty the FFPO cavity before the next pulse burst is launched. Together with the skipped pump cycles in between subsequent bursts, the upper limit of the burst rate amounts to approximately 5 MHz. The feature between two signal pulse sites is an electronic artifact caused by impedance effects in the signal acquisition chain.

As mentioned before, while single pulse bursts can be generated, arbitrary pump-pulse sequences are possible as well. Figure 3(a) depicts a pump-pulse pattern that consists of three individual pulse bursts.

These bursts contain five cycles followed by 13 and 20 cycles. Between the bursts, the AOM suppresses 10 and 20 cycles, respectively. The entire sequence is repeated with a period of 2.3 μs, which corresponds to a sequence repetition rate of approximately 425 kHz. The FFPO signal output at 1410 nm follows the pump sequence with a delay of approximately five laser cycles. Note that the timing offset between pump and signal due to different optical path lengths to the detectors is compensated for in post processing. Figure 3(b) depicts the signal spectrum as well as the corresponding signal output power. Both are measured while the pump sequence shown in Fig. 3(a) is applied. The signal tunability ranges from 1375 to 1835 nm while the burst pattern is preserved. The signal feedback ratio is set to 60% and 20%, respectively. The lowest feedback ratio is reached at 1510 nm (3%). At 1905 nm, the signal time trace cannot be recorded, as the sensitivity of the photodiode (800–1700 nm) decreases drastically. However, comparing the average output power of burst-pattern operation to that of steady-state operation yields a duty cycle of 23%. This suggests that burst operation still works at this wavelength. The average signal output power stated in Fig. 3(b) corresponds to an overall duty cycle of 27%. Exceptions are the operation points at 1375 and 1625 nm, with duty cycles of 20% and 31%, respectively, and the points at 1835 and 1905 nm, with duty cycles of 23%. The maximum output power

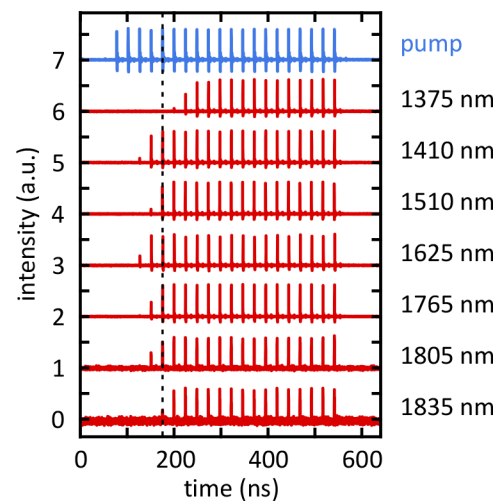


Fig. 4. Signal buildup at different wavelengths. The pump trace corresponds to the 20-cycle burst shown in Fig. 3(a), which starts at approximately 3.4 μs. As a guide to the eye, the dashed line marks the fifth pump cycle. Except at 1375 nm, the signal output reaches its steady-state pulse energy after a maximum of six cycles. Pump power: 680 mW (unmodulated); output coupling ratio: 40–97% (optimized for maximum signal output).

of 39 mW is reached at 1436 nm, and corresponds to a signal pulse energy of 3.6 nJ, measured with a signal feedback ratio of 4%. This corresponds to a photon conversion efficiency of 31%. The output power drops down to the minimum of 1.3 mW (0.14 nJ pulse energy) at 1905 nm, where temporal walk-off between the pump and the signal reduces the gain.

As each individual signal burst emerges from random parametric fluorescence, there is no coherence between individual bursts. However, there is coherence within a signal burst.

Figure 4 depicts the signal buildup cycles at different wavelengths. The pump time trace corresponds to the 20-cycle burst shown in Fig. 3(a), which is launched at approximately 3.4 μs. The signal reaches its steady-state pulse energy within only 4–6 pump cycles. As a guide to the eye, the dashed line marks the temporal position of the fifth pump pulse. Only towards the edges of the tuning range is the buildup time slightly increased.

As mentioned before, no signal ring-down is observed after turning the pump laser off. Thus, burst rates reaching up to the MHz regime can be generated across the entire signal tuning range.

Furthermore, using the idler channel as well would extend the tuning range even further towards the IR.

Higher pump power levels would extend the wavelength range in which the buildup time is retained at five pump cycles. At the same time, the signal buildup would be even faster for the demonstrated wavelengths due to the increased parametric gain. However, the AOM used for this experiment is not optimized for high power throughput. Tight focusing into the AOM crystal to ensure the maximum modulation bandwidth increases the risk of coating damage. Thus, the available pump power at the FFOPO input is set to 680 mW.

In fact, the pump power throughput could be increased by operating the AOM in its zeroth diffraction order, which allows maximum pulse energy transmission. Thereby, the suppression ratio of unwanted pump pulses deteriorates to approximately 80%, given by the AOM diffraction efficiency. However, the FFOPO threshold suppresses the signal output for these pump cycles and thus maintains the excellent pulse contrast ratio.

Conclusion. We have demonstrated a femtosecond FFOPO system in combination with pump pulse picking that enables signal output pulse bursts. Exploiting the high single-pass gain and high intra-cavity losses enables rapid signal buildup and fast off-switching, respectively. This allows burst rates from DC up to 5 MHz to be achieved, as well as arbitrary signal pulse sequences.

Multi-photon direct laser writing applications could greatly benefit from such a system, as photo damage due to heat accumulation could be minimized via burst rate control. At the same time, the wavelength tunability enables the flexible utilization of photoresists with different polymerization activation energies.

Furthermore, stimulated Raman scattering applications and time-resolved photoluminescence measurements will tremendously benefit from wavelength-independent modulation performance. The aforementioned lack of coherence between individual signal bursts does not have any impact on any of these applications.

Our system is superior to fiber supercontinuum sources, which might also cover this spectral range. However, pulse compression after spectral selection would be necessary. Furthermore, the relative intensity noise of these light sources is detrimental

to modulation-based applications, such as stimulated Raman scattering spectroscopy. The FFOPO, on the other hand, preserves the excellent noise performance of the solid-state bulk oscillator [14], which enables measurement sensitivities down to the electronic shot-noise limit.

Funding. European Research Council (PoC 3DPRINTEDOPTICS); Carl-Zeiss-Stiftung; Deutsche Forschungsgemeinschaft (GRK 2642); Center for Integrated Quantum Science and Technology (IQST); Baden-Württemberg Stiftung; Bundesministerium für Bildung und Forschung.

Disclosures. The authors declare no conflicts of interest.

Data availability. Data underlying the results presented in this paper are not publicly available at this time but may be obtained from the authors upon reasonable request.

REFERENCES

1. T. Baldacchini, S. Snider, and R. Zadayan, *Opt. Express* **20**, 29890 (2012).
2. J. Fischer, J. B. Mueller, J. Kaschke, T. J. A. Wolf, A.-N. Unterreiner, and M. Wegener, *Opt. Express* **21**, 26244 (2013).
3. S. M. Eaton, H. Zhang, and P. R. Herman, *Opt. Express* **13**, 4708 (2005).
4. R. R. Gattass, L. R. Cerami, and E. Mazur, *Opt. Express* **14**, 5279 (2006).
5. S. Lévéque-Fort, D. N. Papadopoulos, S. Forget, F. Balembis, and P. Georges, *Opt. Lett.* **30**, 168 (2005).
6. A. Major, V. Barzda, P. A. E. Piunno, S. Musikhin, and U. J. Krull, *Opt. Express* **14**, 5285 (2006).
7. A. Gambetta, V. Kumar, G. Grancini, D. Polli, R. Ramponi, G. Cerullo, and M. Marangoni, *Opt. Lett.* **35**, 226 (2010).
8. W. Min, C. W. Freudiger, S. Lu, and X. S. Xie, *Annu. Rev. Phys. Chem.* **62**, 507 (2011).
9. C. W. Freudiger, W. Yang, G. R. Holtom, N. Peyghambarian, X. S. Xie, and K. Q. Kieu, *Nat. Photonics* **8**, 153 (2014).
10. C. H. Camp and M. T. Cicerone, *Nat. Photonics* **9**, 295 (2015).
11. T. Steinle, V. Kumar, M. Floess, A. Steinmann, M. Marangoni, C. Koch, C. Wege, G. Cerullo, and H. Giessen, *Light: Sci. Appl.* **5**, e16149 (2016).
12. S. Cai, M. Ruan, B. Wu, Y. Shen, and P. Jiang, *IEEE Access* **8**, 64725 (2020).
13. A. Steinmann, B. Metzger, R. Hegenbarth, and H. Giessen, in *CLEO: 2011 - Laser Science to Photonic Applications* (2011), pp. 1–2.
14. T. Steinle, F. Mörz, A. Steinmann, and H. Giessen, *Opt. Lett.* **41**, 4863 (2016).
15. F. Mörz, T. Steinle, A. Steinmann, and H. Giessen, *Opt. Express* **23**, 23960 (2015).